

OpenTrack3D: Towards Accurate and Generalizable Open-Vocabulary 3D Instance Segmentation

Zhishan Zhou¹ Siyuan Wei¹ Zengran Wang¹ Chunjie Wang¹ Xiaosheng Yan¹ Xiao Liu¹
¹PICO, ByteDance, Beijing
{zhouzhishan.2013, weisiyuan.buaa, wangzengran, wangchunjie01, yanxiaosheng, liuxiao.ai}@bytedance.com

Abstract

Generalizing open-vocabulary 3D instance segmentation (OV-3DIS) to diverse, unstructured, and mesh-free environments is crucial for robotics and AR/VR, yet remains a significant challenge. We attribute this to two key limitations of existing methods: (1) proposal generation relies on dataset-specific proposal networks or mesh-based superpoints, rendering them inapplicable in mesh-free scenarios and limiting generalization to novel scenes; and (2) the weak textual reasoning of CLIP-based classifiers, which struggle to recognize compositional and functional user queries. To address these issues, we introduce OpenTrack3D, a generalizable and accurate framework. Unlike methods that rely on pre-generated proposals, OpenTrack3D employs a novel visual-spatial tracker to construct cross-view consistent object proposals online. Given an RGB-D stream, our pipeline first leverages a 2D open-vocabulary segmenter to generate masks, which are lifted to 3D point clouds using depth. Mask-guided instance features are then extracted using DINO feature maps, and our tracker fuses visual and spatial cues to maintain instance consistency. The core pipeline is entirely mesh-free, yet we also provide an optional superpoints refinement module to further enhance performance when scene mesh is available. Finally, we replace CLIP with a multi-modal large language model (MLLM), significantly enhancing compositional reasoning for complex user queries. Extensive experiments on diverse benchmarks, including ScanNet200, Replica, ScanNet++, and SceneFun3D, demonstrate state-of-the-art performance and strong generalization capabilities.

1. Introduction

3D instance segmentation is fundamental to comprehensive scene understanding and underpins applications in VR/AR, robotics, and embodied AI. Unlike single-sensor 2D imaging, precise 3D perception typically depends on calibrated multi-view or RGB-D sensing, which makes large-scale,

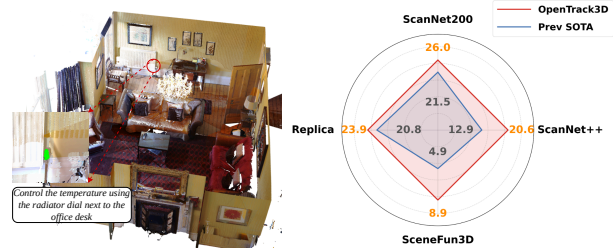


Figure 1. Qualitative and quantitative results of our method. **Left:** Visualization of our results on the **SceneFun3D** dataset. As shown, our method accurately localizes the target objects even under complex query. **Right:** Comparison with prior methods that do not rely on supervised 3D masks, where our approach consistently outperforms them across all benchmarks.

instance-level annotation costly. The resulting scarcity of labeled 3D data remains a central obstacle to advancing robust, deployable 3D perception systems.

Conventional 3D segmentation has therefore concentrated on a limited set of annotated categories, operating in a *closed-vocabulary* regime. Methods span convolutional designs [22, 26, 32, 37] and transformer-based architectures [18, 31], and they process diverse 3D representations—from point clouds and voxels to neural fields [4, 36, 43]. While these systems achieve strong results on benchmarks such as ScanNet200 [30], their practical use is constrained by the small label space and the limited availability of scene-level training data.

To relax vocabulary constraints and better leverage existing priors, recent work explores *open-vocabulary* 3D instance segmentation (OV-3DIS). Many existing solutions are **training-based**, requiring task- or dataset-specific learning to transfer 2D foundation-model knowledge into 3D [2, 8, 9, 12, 13, 27, 39]. Typical pipelines rely on image-bridged supervision, SAM-derived pseudo labels, or distillation from powerful 2D models [17, 20, 28, 29]. This introduces non-trivial training costs, sensitivity to pseudo-label quality, and limited scalability across domains and sensors.

The current generation of training-free OV-3DIS pipelines [1, 14, 24, 35, 38] relies on combining off-the-shelf 2D models with geometric cues, yet their architectures are constrained by inherent limitations. In proposal generation, existing methods fall into two restrictive paradigms: some utilize supervised proposals [1, 14, 27, 35], which inherently restricts the model’s generalization; while others [15, 23, 24, 41, 42] depend on mesh-based superpoints, thereby compromising proposal granularity and becoming inapplicable in mesh-free datasets. Methods [21, 38] avoid the aforementioned issues but yield inferior performance. Concurrently, almost all prior works employ 2D CLIP-based [28] features for classification. This reliance imposes a fundamental limitation, as CLIP lacks the compositional reasoning vital for complex 3D queries.

To address these issues, we introduce **OpenTrack3D**, a generalizable and accurate framework. Unlike methods reliant on supervised 3D proposals or mesh dependencies, OpenTrack3D employs a novel **visual-spatial tracker** to construct cross-view consistent object proposals online from an RGB-D stream. Fig. 2 provides an overview of the design: in **Proposal Generation**, a 2D open-vocabulary detector [3] and SAM [29] produce high-quality masks that are lifted to 3D. Our tracker then fuses visual (DINO features [25]) and spatial cues to maintain instance consistency across views, forming robust track-centric proposals. In **Proposal Refinement**, multi-view consistency filtering suppresses leakage and depth noise, and duplicate hypotheses are merged. Crucially, while the core pipeline is mesh-free, we also provide an **optional Geometry Refinement** to further enhance boundary fidelity when a scene mesh is available. In proposal classification, a small set of informative views per candidate is selected, and a multi-modal large language model (MLLM) is employed for open-vocabulary classification, enabling our system to understand and respond to complex user queries. As shown in Fig. 1, our method achieves state-of-the-art results on multiple benchmarks, including ScanNet200 [6], ScanNet++ [40], Replica [33], and SceneFun3D [7], while demonstrating a strong capability to handle complex, fine-grained queries.

Our contributions are summarized as follows:

- We propose **OpenTrack3D**, a *training-free* framework for OV-3DIS. Its core is a novel **visual-spatial tracker** that generates proposals online by fusing visual and spatial cues, making the approach inherently mesh-free and generalizable.
- We introduce an **MLLM-based** recognition module that leverages top- K informative views for each candidate and performs open-vocabulary classification under a flexible, task-specific label set, enabling robust understanding of complex user queries.
- Our framework achieves **state-of-the-art** results on four

challenging and diverse benchmarks (ScanNet200, ScanNet++, Replica, and SceneFun3D), demonstrating strong generalization and high accuracy.

2. Related Work

Open-Vocabulary 3D Instance Segmentation. Despite remarkable progress in 2D open-vocabulary perception [3, 20], analogous capabilities in 3D remain underexplored. Existing approaches can be broadly categorized into *training-based* and *training-free* paradigms. Training-based methods [2, 8, 9, 12, 13, 27, 39] typically transfer 2D model capabilities into the 3D domain through distillation or pseudo-labeling, but their applicability is often constrained by the scarcity of large-scale 3D annotated data. In contrast, training-free methods mainly differ in how they generate 3D proposals: some rely on closed-vocabulary supervised networks such as [1, 14, 27, 35], while others [15, 23, 24, 41, 42] leverage superpoints extracted from global scene meshes. MaskClustering [38] and OVIR-3D [21] directly reconstruct point-level proposals from individual frames, though their performance remains inferior to the aforementioned counterparts. For open-vocabulary instance classification, most prior works follow OpenMask3D [35], employing CLIP-based representations—typically mask-wise CLIP features in Open3DIS [23] or Alpha-CLIP [34] in Detail Matters [15]. However, these methods are fundamentally limited by CLIP’s semantic capacity. In contrast, our approach leverages an MLLM, offering stronger semantic understanding and broader generalization across diverse and complex 3D scenes.

Functionality and Affordance Segmentation. The task of functionality and affordance segmentation was first introduced by SceneFun3D [7]. Unlike prior datasets such as ScanNet200 [6] and ScanNet++ [40], it requires segmenting extremely small *functional elements*, such as *buttons*, *handles*, and *light switches*. Moreover, the provided textual descriptions are not directly tied to specific object names—for example, queries like “flush the toilet” require the model to possess strong language understanding and reasoning capabilities. SceneFun3D proposed a baseline that trains a specialized Mask3D network on its task-specific training set, and then adopts the CLIP-based classification strategy from OpenMask3D to determine whether each segmented object aligns with the given task description. Fun3DU [5] further introduces a large language model (LLM) to decompose the task into two parts: identifying the *contextual object* (shown in pink) and the *functional object*. It first applies open-vocabulary segmentation to locate the contextual object, and then employs an MLLM to find the corresponding functional object. However, both approaches are designed specifically for the SceneFun3D scenario and fail to generalize effectively to other environments or datasets.

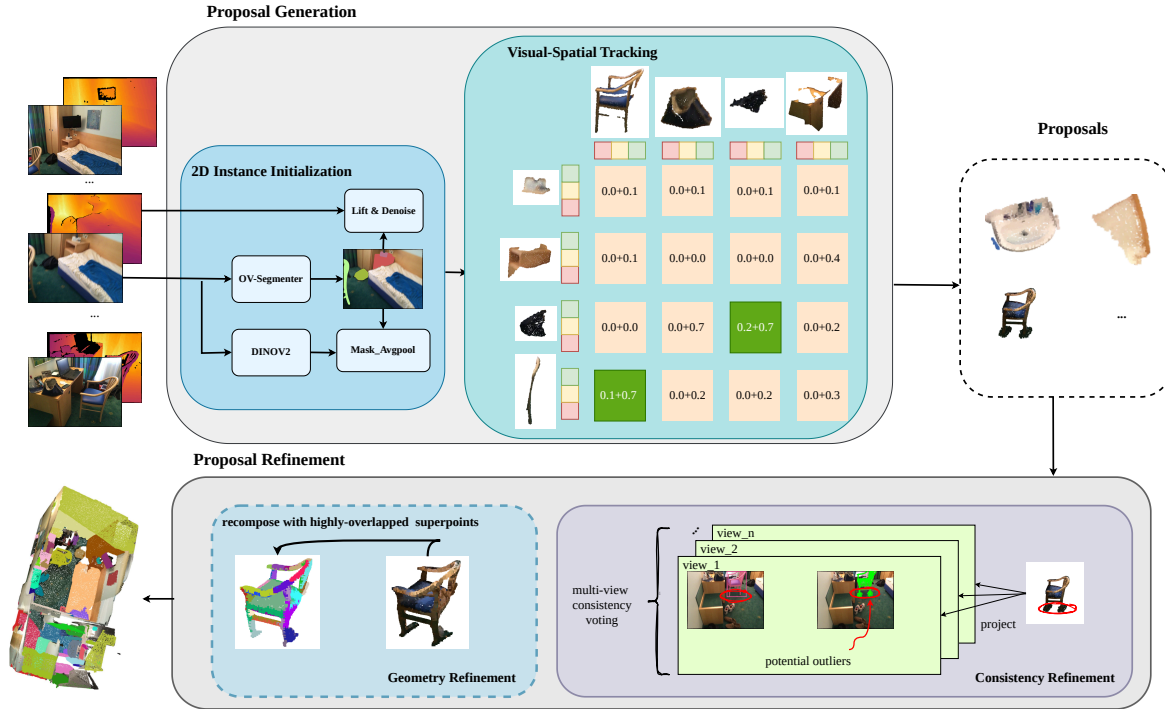


Figure 2. Overview of our **Proposal Generation** and **Proposal Refinement** stages. **Proposal Generation** employs a 2D open-vocabulary segmenter to generate object masks, which are lifted to 3D point clouds using depth maps and subsequently denoised. Mask-guided instance features are extracted from DINO feature maps, and our tracker fuses both visual and spatial cues to maintain instance consistency across frames. **Proposal Refinement** further improves the 3D instances through *Consistency Refinement* and *Geometry Refinement*, while the merging process is omitted for clearer visualization.

3. Method

Problem Formulation Given a multi-view scene observation, composed of a set of T RGB frames $\{I_t\}_{t=1}^T$, their corresponding depth maps $\{D_t\}_{t=1}^T$, camera poses $\{E_t\}_{t=1}^T$, camera intrinsics K , and a pre-reconstructed 3D point cloud P , our goal is to identify and segment a set of 3D instances $\mathcal{O} = \{o_1, o_2, \dots, o_N\} \subset P$ that satisfy a flexible user task description \mathcal{L} . This task \mathcal{L} can range from simple open-set category labels (e.g., "chair, table, etc.") to a complex, arbitrary natural language query (e.g., "Adjust the room's temperature using the radiator dial next to the bed").

Overview We present a unified framework that performs open-vocabulary 3D instance segmentation. Bootstrapped by sparse occupancy and appearance evidence, coarse 3D instances are associated across views through temporal consistency in 3D space; no hand-crafted heuristics are required. The resulting proposals are refined via 2D-3D consistency checks and an optional geometric enhancement step, while duplicate candidates are merged to remove redundancy. Finally, a multi-modal large language

model classifies each instance, delivering accurate open-vocabulary recognition. An overview of our *Proposal Generation* and *Proposal Refinement* stages is shown in Fig. 2.

3.1. Proposal Generation

We introduce a unified design for 3D instance proposal mining from video, consisting of **2D Instance Initialization** and **Visual-Spatial Tracking**. First, **2D Instance Initialization** extracts occupancy and appearance cues from sparse frames and lifts them into coarse 3D instances. Then, **Visual-Spatial Tracking** exploits temporal consistency in 3D occupancy and appearance to associate instances across views, removing the need for hand-crafted heuristics. This streamlined pipeline yields robust instance-level representations without relying on explicit 3D priors.

3.1.1. 2D Instance Initialization

We first harvest 2D instance cues that later guide 3D association. The input video is temporally subsampled to a sparse frame set that still spans the scene while suppressing redundancy. Instance-level cues are gathered in two streams: occupancy and appearance. For occupancy, an open-vocabulary detector proposes, for every frame I_i , a set of bounding boxes $\{b_{i,j}\}$. Each box is forwarded to

SAM to yield a foreground mask $m_{i,j}$. Using calibrated depth D_i , intrinsics K , and camera pose E_i , each box–mask pair is lifted into a coarse 3D point cloud. We then apply DBSCAN [10] to remove noise and recover a clean object-level point cloud $\mathcal{I}_{i,j}$. For appearance, we compute mask-averaged DINO [25] features as the descriptor $\mathbf{f}_{i,j}$.

3.1.2. Visual-Spatial Tracking

Building upon conventional 2D multi-object tracking frameworks, our **Visual-Spatial Tracking** scheme aggregates multi-view information into a unified instance-level representation. Our method jointly exploits temporal consistency by leveraging coherence in both **3D spatial occupancy** and **visual appearance**. By leveraging the natural temporal coherence across frames, the proposed tracking module removes the need for hand-crafted matching rules or label-assignment heuristics.

Each object’s 3D occupancy (the **spatial** cue) is encoded as a coarse voxel grid, and their geometric consistency is measured via an efficient voxel-level IoU metric. Meanwhile, appearance similarity (the **visual** cue) is evaluated using the cosine distance between instance-level feature embeddings. Combining these two cues, the pairwise similarity score between a new instance $\mathcal{I}_{i,*}$ and an active track $\mathcal{T}_{(i-1)}$ is formulated as

$$s = \alpha \cos(\mathbf{f}_T, \mathbf{f}_I) + (1 - \alpha) \text{IoU}^{\text{voxel}}(\mathcal{I}_{i,*}, \mathcal{T}_{(i-1)}), \quad (1)$$

where α balances the influence of appearance and occupancy similarity, and $\mathbf{f}_T, \mathbf{f}_I$ denote the feature embeddings of $\mathcal{T}_{(i-1)}$ and $\mathcal{I}_{i,*}$, respectively. As illustrated in Fig. 2, even when the reconstructed chair point cloud of a new frame yields a low voxel IoU, the strong visual similarity captured by DINO features still enables correct association; conversely, two spatially separated backpacks may share high visual similarity, yet the IoU term effectively disambiguates them by enforcing geometric coherence.

During online tracking, each tracklet’s voxel representation is incrementally updated by merging the voxels of its newly matched detection, while its DINOv2-based descriptor is refreshed via an Exponential Moving Average. The bipartite association between instances and existing tracks is then solved using the Hungarian algorithm. After association, a match is considered successful if its similarity score exceeds a threshold τ_{match} ; otherwise, the unmatched instance initializes a new tracklet.

3.2. Proposal Refinement

After Visual-Spatial Tracking, we obtain the coarse 3D proposals \mathcal{P}_k for each tracked instance k . These proposals are initially formed by aggregating the frame-wise point clouds and matching them to the global scene point cloud \mathcal{P} via K -nearest neighbors (KNN) association. However, due to

the inherent mismatch between the temporally lifted frame-wise instances and the static scene representation, coupled with potential registration errors and accumulated depth noise, the resulting proposal \mathcal{P}_k often contains significant noise and outliers. Therefore, a meticulously designed refinement stage is crucial to achieving accurate and clean 3D instance boundaries.

3.2.1. Consistency Refinement

Due to the inherent mismatch during frame-to-scene aggregation, \mathcal{P}_k often suffers from partially missed or thin structures. To address this, we first optionally perform a point cloud expansion on \mathcal{P}_k : we incorporate neighboring points from the global scene \mathcal{P} within a distance τ_{exp} to form an expanded candidate set \mathcal{P}'_k .

Then, we propose Consistency Refinement which is designed to eliminate noisy points from this expanded set \mathcal{P}'_k by leveraging a 2D-3D consistency metric, derived from projection and multi-view voting. Specifically, for a given object’s expanded point cloud \mathcal{P}'_k , we project it onto 2D image planes and evaluate the 2D-3D consistency score s_j of each 3D point $p_j \in \mathcal{P}'_k$ by verifying whether the projected coordinate lies within the corresponding 2D instance mask of each visible view (i.e., views where the point projects onto the image canvas) and computing the average voting score as follows:

$$s_j = \frac{1}{|I_{\text{vis}}^{p_j}|} \sum_{i \in I_{\text{vis}}^{p_j}} \mathbb{I}[\pi_i(p_j) \in m_{i,k}] \quad (2)$$

where $I_{\text{vis}}^{p_j}$ denotes the set of visible frame indices for point p_j . The function $\pi_i(\cdot)$ represents the projection from the world coordinate system to the 2D image plane of the i -th frame, and $\mathbb{I}(\cdot)$ is the indicator function. Ultimately, we filter out noisy points with consistency scores below the threshold τ_{vis} and retain the remaining ones, $\mathcal{P}_k^{\text{cr}} = \{p_j \in \mathcal{P}'_k \mid s_j \geq \tau_{\text{vis}}\}$, as the denoised and structurally complete object point cloud.

3.2.2. Optional Geometry Refinement

After Consistency Refinement, boundaries may still look ragged or extend onto large planar regions due to mask leakage and depth noise. To enhance geometric coherence further, we introduce an optional Geometry Refinement that leverages superpoints [11].

In general, we utilize a set of instance-associated superpoints for the instance re-composition. More specifically, for each superpoint \mathcal{S}_j , if the proportion of its constituent points contained in $\mathcal{P}_k^{\text{cr}}$ exceeds the threshold γ , the superpoint \mathcal{S}_j is incorporated into the reconstructed instance $\mathcal{P}_k^{\text{gr}}$, as formalized in Equation 3.

$$\mathcal{P}_k^{\text{gr}} = \{\mathcal{S}_j \in \mathcal{S} \mid \frac{|\mathcal{S}_j \cap \mathcal{P}_k^{\text{cr}}|}{|\mathcal{S}_j|} \geq \gamma\} \quad (3)$$

Method	Supervised 3D Mask	ScanNet200			Replica		
		AP	AP ₅₀	AP ₂₅	AP	AP ₅₀	AP ₂₅
Mask3D [31](Closed-vocabulary)	-	26.9	36.2	41.4	-	-	-
OpenIns3D [14]	✓	8.8	10.3	14.4	-	-	-
OpenScene [27]	✓	11.7	15.2	17.8	-	-	-
OpenMask3D [35]	✓	15.4	19.9	23.1	13.1	18.4	24.2
Open3DIS* [23]	✓	23.7	29.4	32.8	18.4	23.8	28.2
Any3DIS* [24]	✓	25.8	-	-	-	-	-
OpenYOLO3D [1]	✓	21.9	28.3	31.7	23.7	28.6	34.8
Detail Matters [15]	✓	25.8	32.5	36.2	22.6	31.7	37.7
SAM3D [12]	×	9.8	15.2	20.7	-	-	-
OVIR-3D [21]	×	9.3	18.7	25.0	11.0	20.5	27.5
MaskClustering [38]	×	12.0	23.3	30.1	-	-	-
SAI3D [41]	×	12.7	18.8	24.1	-	-	-
SAM2Objects [42]	×	13.3	19.0	23.8	-	-	-
Open3DIS* [23]	×	18.2	26.1	31.4	18.2	25.9	31.0
Any3DIS* [24]	×	19.1	-	-	-	-	-
Detail Matters[15]	×	21.5	31.2	37.7	20.8	32.4	38.5
Ours	×	26.0	37.7	45.4	23.9	36.4	47.6

Table 1. Results on **ScanNet200** validation set and Replica dataset. Bold entries indicate best performance. Compared with methods that do not rely on supervised 3D masks, our approach achieves superior results, especially in terms of AP₅₀ and AP₂₅.

3.2.3. Proposal Merging

Tracking and lifting can produce duplicate or highly overlapping hypotheses for the same object (e.g., occlusions or short-track fragmentation). We resolve redundancies by merging instances based on voxel-point-set overlap, following a standard non-maximum suppression (NMS) pipeline. Each track’s length serves as its objectness score, and tracks are sorted accordingly. For each track, we compute the voxel-point-set IoU with previously retained objects. If the IoU exceeds a threshold τ_{merge} , the track is considered redundant—likely from fragmented observations of the same object—and its points are merged into the existing object.

3.3. Proposal Classification

Previous open-vocabulary approaches typically use CLIP to associate textual queries with candidate proposals. However, the limited pre-training objective and scale of CLIP constrain its ability to reason over fine-grained categories or complex textual descriptions. This limitation constitutes a major bottleneck in open-vocabulary perception.

To address this issue, we employ multi-modal large language model (MLLM) for the final classification stage. To keep computation efficient, we leverage the tracklets established earlier and select a compact set of representative frames for each object.

Specifically, we rank all camera views by the fraction of the object’s reconstructed point cloud that falls within each camera frustum. Ties are broken using the projected mask area in the image, favoring views that observe the object

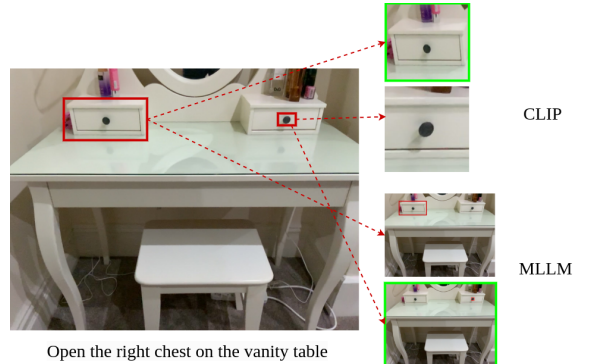


Figure 3. Comparison of CLIP and MLLM on fine-grained, complex textual queries. CLIP receives cropped object regions, while MLLM processes the full image with the target highlighted by a red box. Green boxes indicate predicted instances for each method. MLLM better captures complex descriptions and produces more accurate predictions, whereas CLIP often fails.

frontally and at close range. As illustrated in Fig. 3, we select the top-K views for each object and feed them into the MLLM. Each input consists of the full image where the target object is highlighted by a red bounding box. The MLLM is prompted to determine whether the highlighted instance belongs to any category in the restricted label set \mathcal{C} , or semantically matches a user-provided textual description. By jointly reasoning over the top-K representative images, the model achieves more robust and context-aware classification.

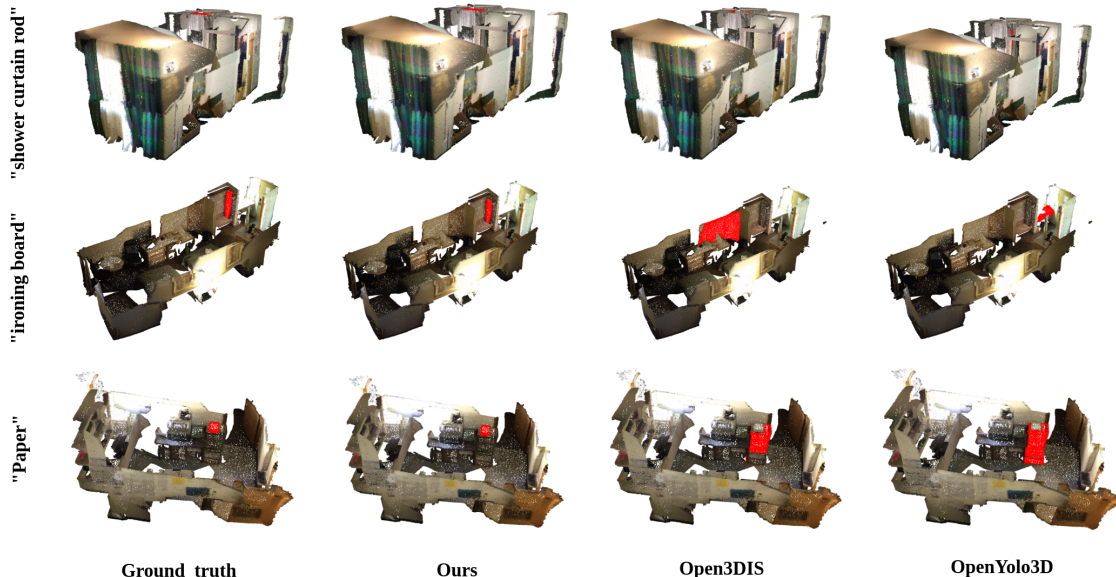


Figure 4. Comparative Visualization of Open-Vocabulary 3D Instance Segmentation on ScanNet200. Red masks denote query-correlated 3D instances. The comparative results demonstrate our method’s clear advantage in addressing long-tail categories, showcasing improved segmentation accuracy and robustness when compared to baseline approaches.

4. Experiments

4.1. Experimental Setup

Datasets We first evaluate our method on the widely used open-vocabulary 3D instance segmentation benchmarks ScanNet200 [6] and Replica [33], enabling fair comparisons with existing approaches. The ScanNet200 validation set consists of 312 scenes spanning 200 object categories, while Replica is a synthetic dataset comprising 8 scenes with 48 categories. Both datasets exhibit similar point cloud distributions and category distributions across scenes. Furthermore, to thoroughly assess the generalizability of our approach, we extend our evaluation to ScanNet++ [40] and SceneFun3D [7]—two benchmarks that present substantially different and more challenging conditions. ScanNet++ provides increased complexity with 50 meticulously annotated scenes containing 1,554 fine-grained semantic labels. SceneFun3D challenges methods to perform language-guided segmentation of functional elements based on complex textual descriptions. It provides highly fine-grained annotations, including handles and buttons, and consists of 30 validation and 85 test scenes.

Metrics Our evaluation employs the standard average precision (AP) metrics: AP (computed across IoU thresholds from 0.5 to 0.95 with 0.05 increments), AP₅₀ (at an IoU threshold of 0.5), and AP₂₅ (at an IoU threshold of 0.25). Notably, we report results under the Top-1 evaluation protocol, as it aligns more closely with real-world application

scenarios. Results obtained using the Top-k evaluation protocol—where each instance can have multiple predicted categories and the final result is derived from the top 300/600 predictions—are marked with an *.

Implementation Details For the ScanNet200 and ScanNet++ datasets, we follow prior works and downsample the RGB-D frames by factors of 5 and 10, respectively. We employ YOLO-World-X [3] and SAM2-Large [29] as our open-vocabulary segmenter, and use DINOv2-Base as the backbone for semantic feature extraction. For the MLLM, we adopt Qwen3-VL-4B, which provides a favorable balance between performance and inference efficiency. For all benchmarks, we use the same hyperparameters for proposal generation, with τ_{match} set to 0.4 and α set to 0.5. For proposal refinement, we default to $\tau_{\text{exp}} = 0.03$ m, $\tau_{\text{vis}} = 0.1$, $\tau_{\text{merge}} = 0.6$ and $\gamma = 0.3$. For datasets where most objects are fully visible in the camera views, such as SceneFun3D, we adopt $\tau_{\text{exp}} = 0$ and a higher threshold of $\tau_{\text{vis}} = 0.8$. In addition, for the MLLM parameter K , we use $K = 3$ on ScanNet200 and $K = 1$ for all other datasets. More implementation details and ablation studies on hyperparameter sensitivity are provided in the supplementary material.

4.2. Main Results

Results on ScanNet200 and Replica To ensure fair benchmarking against existing open-vocabulary 3D instance segmentation approaches, we perform comparative experiments on the ScanNet200 and Replica datasets.



Figure 5. Qualitative Results on ScanNet++ (left) and SceneFun3D (right). We demonstrate instance segmentation results for various text queries. The visualizations demonstrate our method’s capability to delineate objects with arbitrary geometries while maintaining recognition accuracy for specific textual descriptions.

Quantitative results are presented in Table 1, and qualitative comparisons on ScanNet200 are shown in Fig. 4. Our method establishes a new state-of-the-art among open-vocabulary 3D instance segmentation approaches. When compared with methods that do not rely on supervised 3D masks from pre-trained models, our approach surpasses all previous SOTA results by a large margin, especially in terms of AP_{50} and AP_{25} . On **ScanNet200**, we outperform the previous best by 6.5% and 8.3%, while on **Replica**, the improvements reach 4.0% and 9.1%, respectively. These results demonstrate that our generalizable framework consistently achieves significant advantages even on standard benchmarks.

Method	AP	AP_{50}	AP_{25}
Segment3D [13]	10.1	17.7	20.2
Open3DIS [23]	11.9	18.1	21.7
Any3DIS [24]	12.9	19.0	21.9
Ours	20.6	34.2	43.4

Table 2. Results on the ScanNet++ dataset, evaluated on a subset of 100 classes.

Results on ScanNet++ and SceneFun3D To further validate the generalization of our method, we conduct additional experiments on the challenging ScanNet++ and SceneFun3D datasets. For ScanNet++, we follow Any3DIS [24] by benchmarking a subset of 100 classes. Quantitative results are presented in Table 2 while Table 3, and qualitative comparisons are shown in Fig. 5. Our method achieves a substantial improvement of 8.3% in AP over the previous state-of-the-art method Any3DIS on ScanNet++. On SceneFun3D, our approach outperforms OpenMask3D-F, which relies on supervised 3D proposals trained on SceneFun3D. Compared to Fun3DU, which also leverages MLLMs, our method achieves a 5.3% improvement. Compared with ScanNet200 and Replica, both

Method	AP_{50}	AP_{25}
OpenMask3D [35]	0.0	0.0
LERF [16]	4.9	11.3
OpenMask3D-F [7]	8.0	17.5
Fun3DU [5]	3.6	8.8
Ours	8.9	18.5

Table 3. Results on the SceneFun3D test dataset. The reported Fun3DU results are obtained from the publicly available hidden test benchmark provided by SceneFun3D.

ScanNet++ and SceneFun3D present greater challenges due to their larger-scale point clouds and finer-grained object categories. For instance, the Mask3D network trained on ScanNet200 fails to generalize to ScanNet++, while SceneFun3D is a mesh-free dataset where superpoint-based proposal generation methods are inapplicable. These results collectively demonstrate the strong **accuracy** and **generalization** of our approach across diverse and challenging 3D benchmarks.

4.3. Ablation Study

Ablation Study on Proposal Generation. We conduct ablation studies on the proposal generation stage to evaluate the contribution of different components. As shown in Table 5, combining both the DINO score and the IoU score yields the best overall performance. Using only the visual (DINO) score tends to merge distinct objects with similar semantics (e.g., two spatially separated chairs) into a single track, reducing tracking precision. In contrast, relying solely on the IoU score requires setting an excessively high threshold to prevent merging adjacent instances, which in turn hampers cross-frame tracking. We further compare extracting DINO features from bounding boxes rather than instance masks. The results show that bbox-wise features lead to noticeable degradation, likely due to the inclusion of background noise and reduced robustness to occlusion. In

method	ScanNet200			Replica			ScanNet++			SceneFun3D	
	AP	AP ₅₀	AP ₂₅	AP	AP ₅₀	AP ₂₅	AP	AP ₅₀	AP ₂₅	AP ₅₀	AP ₂₅
CLIP	22.9	33.4	39.8	22.1	32.2	39.6	18.5	31.1	41.2	4.0	8.7
MLLM	26.0	37.7	45.4	23.9	36.4	47.6	20.6	34.2	43.4	9.8	20.6

Table 4. Comparison between CLIP and multi-modal large language model (MLLM) classifiers on the validation sets of ScanNet200, Replica, ScanNet++, and SceneFun3D.

Method	AP	AP ₅₀	AP ₂₅
Baseline	28.6	40.5	48.8
w/o IoU score	26.0	38.0	44.1
w/o DINO score	26.3	37.9	46.8
w/o denoise	27.8	39.8	46.9
w/o mask-wise feature	27.5	38.3	46.3

Table 5. Ablation study on proposal generation evaluated on a subset of the ScanNet200 validation set.

addition, removing the denoising step on frame-wise point clouds also results in a clear performance drop, highlighting that cleaner per-frame proposals positively impact both tracking and segmentation accuracy.

Ablation Study on MLLM To validate the effectiveness of employing a multi-modal large language model (MLLM) as the classifier, we compare it with the CLIP-based baseline used in prior works. Following OpenMask3D, we select the top-5 views per instance and extract multi-scale CLIP features, which are then averaged to form the final representation. As shown in Table 4, replacing CLIP with an MLLM consistently improves performance across all datasets. The gain is particularly pronounced on SceneFun3D, where fine-grained textual understanding is required. In such scenarios, the MLLM demonstrates a superior capacity for semantic reasoning compared to CLIP. Moreover, even compared to the recent state-of-the-art method [15], which employs Alpha-CLIP and aggregates top-20 or top-40 view features, our simple MLLM-based classifier achieves superior results, demonstrating both higher effectiveness and efficiency.

Ablation Study on Proposal Refinement As shown in Table 6, our refinement module consistently improves performance across different datasets. In particular, for the SceneFun3D dataset, which mainly consists of small and fine-grained categories such as *buttons* and *handles*, even a single inaccurate segmentation within a track can significantly degrade performance, making the proposed Consistency Refinement module essential. For ScanNet200, the most notable improvements appear in AP and AP₅₀, indicating that while our tracking framework achieves high recall, its precision remains limited without refinement. To further

Method	ScanNet200			SceneFun3D	
	AP	AP ₅₀	AP ₂₅	AP ₅₀	AP ₂₅
Baseline	14.2	31.4	46.5	2.0	7.0
+ CR	17.3	33.2	47.1	9.5	20.1
+ GR	27.0	37.1	44.6	-	-
+ Merge	28.6	40.5	48.8	9.8	20.6

Table 6. Ablation study on proposal refinement on subsets of the ScanNet200 and SceneFun3D validation sets. CR: Consistency Refinement. GR: Geometry Refinement. For SceneFun3D, which does not provide mesh geometry, the GR module is omitted.

enhance precision, we incorporate superpoints—derived from mesh geometry—into the refinement stage. This addition helps produce more spatially coherent instance masks on datasets with mesh. Importantly, our framework remains compatible with mesh-free datasets such as SceneFun3D, where the superpoint-based refinement can be disabled without affecting the overall pipeline. Finally, as shown in the results, proposal merging and filtering play a minor role for SceneFun3D. This is likely because most small objects remain visible across consecutive frames, and our tracking module rarely produces fragmented tracklets, making such merging unnecessary.

5. Limitation and Conclusion

Despite achieving state-of-the-art results, OpenTrack3D remains limited by its dependence on video quality and the noise introduced during 2D-to-3D lifting. Imperfect camera poses or depth maps can impair accurate 3D localization and cross-view consistency.

Looking ahead, we aim for two primary extensions. First, we will enhance the robustness of the lifting stage by integrating more advanced, unified 2D foundation models. Second, leveraging OpenTrack3D’s demonstrated strong generalization capability, we envision applying our framework as a cost-effective tool for large-scale, open-vocabulary 3D data annotation. This line of research will ultimately accelerate the development of 3D-native open-vocabulary foundation models, bridging the current gap between generalized 2D and 3D vision.

References

- [1] Mohamed El Amine Boudjoghra, Angela Dai, Jean Lahoud, Hisham Cholakkal, Rao Muhammad Anwer, Salman Khan, and Fahad Shahbaz Khan. Open-yolo 3d: Towards fast and accurate open-vocabulary 3d instance segmentation. *arXiv preprint arXiv:2406.02548*, 2024. 2, 5
- [2] Runnan Chen, Youquan Liu, Lingdong Kong, Xinge Zhu, Yuexin Ma, Yikang Li, Yuenan Hou, Yu Qiao, and Wenping Wang. Clip2scene: Towards label-efficient 3d scene understanding by clip. In *Proceedings of the IEEE/CVF Conference on Computer Vision and Pattern Recognition*, pages 7020–7030, 2023. 1, 2
- [3] Tianheng Cheng, Lin Song, Yixiao Ge, Wenyu Liu, Xingang Wang, and Ying Shan. Yolo-world: Real-time open-vocabulary object detection. In *Proceedings of the IEEE/CVF Conference on Computer Vision and Pattern Recognition*, pages 16901–16911, 2024. 2, 6, 1
- [4] Zi-Ting Chou, Sheng-Yu Huang, I Liu, Yu-Chiang Frank Wang, et al. Gsnerf: Generalizable semantic neural radiance fields with enhanced 3d scene understanding. In *Proceedings of the IEEE/CVF Conference on Computer Vision and Pattern Recognition*, pages 20806–20815, 2024. 1
- [5] Jaime Corsetti, Francesco Giuliari, Alice Fasoli, Davide Boscaini, and Fabio Poiesi. Functionality understanding and segmentation in 3d scenes. In *Proceedings of the Computer Vision and Pattern Recognition Conference*, pages 24550–24559, 2025. 2, 7
- [6] Angela Dai, Angel X. Chang, Manolis Savva, Maciej Halber, Thomas Funkhouser, and Matthias Nießner. Scannet: Richly-annotated 3d reconstructions of indoor scenes. In *Proc. Computer Vision and Pattern Recognition (CVPR), IEEE*, 2017. 2, 6, 1
- [7] Alexandros Delitzas, Ayca Takmaz, Federico Tombari, Robert Sumner, Marc Pollefeys, and Francis Engelmann. Scenefun3d: Fine-grained functionality and affordance understanding in 3d scenes. In *Proceedings of the IEEE/CVF Conference on Computer Vision and Pattern Recognition*, pages 14531–14542, 2024. 2, 6, 7, 1
- [8] Runyu Ding, Jihan Yang, Chuhui Xue, Wenqing Zhang, Song Bai, and Xiaojuan Qi. Lowis3d: Language-driven open-world instance-level 3d scene understanding. *IEEE Transactions on Pattern Analysis and Machine Intelligence*, 2023. 1, 2
- [9] Runyu Ding, Jihan Yang, Chuhui Xue, Wenqing Zhang, Song Bai, and Xiaojuan Qi. Pla: Language-driven open-vocabulary 3d scene understanding. In *Proceedings of the IEEE/CVF conference on computer vision and pattern recognition*, pages 7010–7019, 2023. 1, 2
- [10] Martin Ester, Hans-Peter Kriegel, Jörg Sander, Xiaowei Xu, et al. A density-based algorithm for discovering clusters in large spatial databases with noise. In *kdd*, pages 226–231, 1996. 4
- [11] Pedro F Felzenszwalb and Daniel P Huttenlocher. Efficient graph-based image segmentation. *International journal of computer vision*, 59:167–181, 2004. 4
- [12] Haoyu Guo, He Zhu, Sida Peng, Yuang Wang, Yujun Shen, Ruizhen Hu, and Xiaowei Zhou. Sam-guided graph cut for 3d instance segmentation. In *European Conference on Computer Vision*, pages 234–251. Springer, 2024. 1, 2, 5
- [13] Rui Huang, Songyou Peng, Ayca Takmaz, Federico Tombari, Marc Pollefeys, Shiji Song, Gao Huang, and Francis Engelmann. Segment3d: Learning fine-grained class-agnostic 3d segmentation without manual labels. In *European Conference on Computer Vision*, pages 278–295. Springer, 2024. 1, 2, 7
- [14] Zhening Huang, Xiaoyang Wu, Xi Chen, Hengshuang Zhao, Lei Zhu, and Joan Lasenby. Openins3d: Snap and lookup for 3d open-vocabulary instance segmentation. In *European Conference on Computer Vision*, pages 169–185. Springer, 2024. 2, 5
- [15] Sanghun Jung, Jingjing Zheng, Ke Zhang, Nan Qiao, Albert YC Chen, Lu Xia, Chi Liu, Yuyin Sun, Xiao Zeng, Hsiang-Wei Huang, et al. Details matter for indoor open-vocabulary 3d instance segmentation. In *Proceedings of the IEEE/CVF International Conference on Computer Vision*, pages 9627–9637, 2025. 2, 5, 8, 1
- [16] Justin Kerr, Chung Min Kim, Ken Goldberg, Angjoo Kanazawa, and Matthew Tancik. Lrf: Language embedded radiance fields. In *Proceedings of the IEEE/CVF international conference on computer vision*, pages 19729–19739, 2023. 7
- [17] Alexander Kirillov, Eric Mintun, Nikhila Ravi, Hanzi Mao, Chloe Rolland, Laura Gustafson, Tete Xiao, Spencer Whitehead, Alexander C Berg, Wan-Yen Lo, et al. Segment anything. In *Proceedings of the IEEE/CVF International Conference on Computer Vision*, pages 4015–4026, 2023. 1
- [18] Maxim Kolodiaznyi, Anna Vorontsova, Anton Konushin, and Danila Rukhovich. Oneformer3d: One transformer for unified point cloud segmentation. In *Proceedings of the IEEE/CVF Conference on Computer Vision and Pattern Recognition*, pages 20943–20953, 2024. 1
- [19] Woosuk Kwon, Zhuohan Li, Siyuan Zhuang, Ying Sheng, Lianmin Zheng, Cody Hao Yu, Joseph E. Gonzalez, Hao Zhang, and Ion Stoica. Efficient memory management for large language model serving with pagedattention. In *Proceedings of the ACM SIGOPS 29th Symposium on Operating Systems Principles*, 2023. 1
- [20] Shilong Liu, Zhaoyang Zeng, Tianhe Ren, Feng Li, Hao Zhang, Jie Yang, Qing Jiang, Chunyuan Li, Jianwei Yang, Hang Su, Jun Zhu, and Lei Zhang. Grounding dino: Marrying dino with grounded pre-training for open-set object detection, 2024. 1, 2
- [21] Shiyang Lu, Haonan Chang, Eric Pu Jing, Abdeslam Boularias, and Kostas Bekris. Ovir-3d: Open-vocabulary 3d instance retrieval without training on 3d data. In *Conference on Robot Learning*, pages 1610–1620. PMLR, 2023. 2, 5
- [22] Tuan Duc Ngo, Binh-Son Hua, and Khoi Nguyen. Isbnet: a 3d point cloud instance segmentation network with instance-aware sampling and box-aware dynamic convolution. In *Proceedings of the IEEE/CVF Conference on Computer Vision and Pattern Recognition*, pages 13550–13559, 2023. 1
- [23] Phuc Nguyen, Tuan Duc Ngo, Evangelos Kalogerakis, Chuang Gan, Anh Tran, Cuong Pham, and Khoi Nguyen. Open3dis: Open-vocabulary 3d instance segmentation with

- 2d mask guidance. In *Proceedings of the IEEE/CVF Conference on Computer Vision and Pattern Recognition*, pages 4018–4028, 2024. 2, 5, 7, 1
- [24] Phuc Nguyen, Minh Luu, Anh Tran, Cuong Pham, and Khoi Nguyen. Any3dis: Class-agnostic 3d instance segmentation by 2d mask tracking. In *Proceedings of the Computer Vision and Pattern Recognition Conference*, pages 3636–3645, 2025. 2, 5, 7
- [25] Maxime Oquab, Timothée Darcet, Théo Moutakanni, Huy Vo, Marc Szafraniec, Vasil Khalidov, Pierre Fernandez, Daniel Haziza, Francisco Massa, Alaaeldin El-Nouby, et al. Dinov2: Learning robust visual features without supervision. *arXiv preprint arXiv:2304.07193*, 2023. 2, 4, 1
- [26] Bohao Peng, Xiaoyang Wu, Li Jiang, Yukang Chen, Hengshuang Zhao, Zhuotao Tian, and Jiaya Jia. Oa-cnns: Omni-adaptive sparse cnns for 3d semantic segmentation. In *Proceedings of the IEEE/CVF Conference on Computer Vision and Pattern Recognition*, pages 21305–21315, 2024. 1
- [27] Songyou Peng, Kyle Genova, Chiyu Jiang, Andrea Tagliasacchi, Marc Pollefeys, Thomas Funkhouser, et al. Openscene: 3d scene understanding with open vocabularies. In *Proceedings of the IEEE/CVF conference on computer vision and pattern recognition*, pages 815–824, 2023. 1, 2, 5
- [28] Alec Radford, Jong Wook Kim, Chris Hallacy, Aditya Ramesh, Gabriel Goh, Sandhini Agarwal, Girish Sastry, Amanda Askell, Pamela Mishkin, Jack Clark, et al. Learning transferable visual models from natural language supervision. In *International conference on machine learning*, pages 8748–8763. PMLR, 2021. 1, 2
- [29] Nikhila Ravi, Valentin Gabeur, Yuan-Ting Hu, Ronghang Hu, Chaitanya Ryali, Tengyu Ma, Haitham Khedr, Roman Rädle, Chloe Rolland, Laura Gustafson, et al. Sam 2: Segment anything in images and videos. *arXiv preprint arXiv:2408.00714*, 2024. 1, 2, 6
- [30] David Rozenberszki, Or Litany, and Angela Dai. Language-grounded indoor 3d semantic segmentation in the wild. In *European conference on computer vision*, pages 125–141. Springer, 2022. 1
- [31] Jonas Schult, Francis Engelmann, Alexander Hermans, Or Litany, Siyu Tang, and Bastian Leibe. Mask3d: Mask transformer for 3d semantic instance segmentation. *arXiv preprint arXiv:2210.03105*, 2022. 1, 5
- [32] Sangyun Shin, Kaichen Zhou, Madhu Vankadari, Andrew Markham, and Niki Trigoni. Spherical mask: Coarse-to-fine 3d point cloud instance segmentation with spherical representation. In *Proceedings of the IEEE/CVF Conference on Computer Vision and Pattern Recognition*, pages 4060–4069, 2024. 1
- [33] Julian Straub, Thomas Whelan, Lingni Ma, Yufan Chen, Erik Wijmans, Simon Green, Jakob J. Engel, Raul Mur-Artal, Carl Ren, Shobhit Verma, Anton Clarkson, Mingfei Yan, Brian Budge, Yajie Yan, Xiaqing Pan, June Yon, Yuyang Zou, Kimberly Leon, Nigel Carter, Jesus Briales, Tyler Gillingham, Elias Mueggler, Luis Pesqueira, Manolis Savva, Dhruv Batra, Hauke M. Strasdat, Renzo De Nardi, Michael Goesele, Steven Lovegrove, and Richard Newcombe. The Replica dataset: A digital replica of indoor spaces. *arXiv preprint arXiv:1906.05797*, 2019. 2, 6, 1
- [34] Zeyi Sun, Ye Fang, Tong Wu, Pan Zhang, Yuhang Zang, Shu Kong, Yuanjun Xiong, Dahua Lin, and Jiaqi Wang. Alpha-clip: A clip model focusing on wherever you want. In *Proceedings of the IEEE/CVF conference on computer vision and pattern recognition*, pages 13019–13029, 2024. 2
- [35] Ayça Takmaz, Elisabetta Fedele, Robert W Sumner, Marc Pollefeys, Federico Tombari, and Francis Engelmann. Open-mask3d: Open-vocabulary 3d instance segmentation. *arXiv preprint arXiv:2306.13631*, 2023. 2, 5, 7
- [36] Suhani Vora, Noha Radwan, Klaus Greff, Henning Meyer, Kyle Genova, Mehdi SM Sajjadi, Etienne Pot, Andrea Tagliasacchi, and Daniel Duckworth. Nesf: Neural semantic fields for generalizable semantic segmentation of 3d scenes. *arXiv preprint arXiv:2111.13260*, 2021. 1
- [37] Thang Vu, Kookhoi Kim, Tung M Luu, Thanh Nguyen, and Chang D Yoo. Softgroup for 3d instance segmentation on point clouds. In *Proceedings of the IEEE/CVF Conference on Computer Vision and Pattern Recognition*, pages 2708–2717, 2022. 1
- [38] Mi Yan, Jiazhao Zhang, Yan Zhu, and He Wang. Maskclustering: View consensus based mask graph clustering for open-vocabulary 3d instance segmentation. In *Proceedings of the IEEE/CVF Conference on Computer Vision and Pattern Recognition*, pages 28274–28284, 2024. 2, 5
- [39] Jihan Yang, Runyu Ding, Weipeng Deng, Zhe Wang, and Xiaojuan Qi. Regionplc: Regional point-language contrastive learning for open-world 3d scene understanding. In *Proceedings of the IEEE/CVF conference on computer vision and pattern recognition*, pages 19823–19832, 2024. 1, 2
- [40] Chandan Yeshwanth, Yueh-Cheng Liu, Matthias Nießner, and Angela Dai. Scannet++: A high-fidelity dataset of 3d indoor scenes, 2023. 2, 6, 1
- [41] Yingda Yin, Yuzheng Liu, Yang Xiao, Daniel Cohen-Or, Jingwei Huang, and Baoquan Chen. Sai3d: Segment any instance in 3d scenes. In *Proceedings of the IEEE/CVF Conference on Computer Vision and Pattern Recognition*, pages 3292–3302, 2024. 2, 5
- [42] Jihuai Zhao, Junbao Zhuo, Jiansheng Chen, and Huimin Ma. Sam2object: Consolidating view consistency via sam2 for zero-shot 3d instance segmentation. In *Proceedings of the Computer Vision and Pattern Recognition Conference*, pages 19325–19334, 2025. 2, 5
- [43] Shuaifeng Zhi, Tristan Laidlow, Stefan Leutenegger, and Andrew J Davison. In-place scene labelling and understanding with implicit scene representation. In *Proceedings of the IEEE/CVF International Conference on Computer Vision*, pages 15838–15847, 2021. 1

OpenTrack3D: Towards Accurate and Generalizable Open-Vocabulary 3D Instance Segmentation

Supplementary Material

6. More Implementation Details

In this section, we provide additional implementation details of our MLLM components to improve understanding and reproducibility. We deploy Qwen3-4B using vLLM [19] on a single A100 GPU and use the default generation settings unless otherwise noted.

For the SceneFun3D [7] dataset, the user-provided task descriptions cannot be directly processed by open-vocabulary detectors. To bridge this gap, we use the same MLLM to convert each textual query into a list of directly operable affordance nouns using the following prompt: Extract directly operable affordance elements from the given task description (e.g., handle, knob, switch, latch, lever). Do not include whole objects. Output a comma-separated list of nouns. Task: {}. These extracted nouns are then fed into the open-vocabulary detector.

For datasets [6, 33, 40] with predefined category sets, we adopt a unified prompt template: Identify the object shown in the red rectangle. Return the class name from {}. If no object is shown, return 'none'. In contrast, for SceneFun3D, we employ a specialized prompt that maps all task descriptions in a scene to their corresponding task indices in a single forward pass: The interactive element is shown in the red rectangle. Determine whether the element in the image can accomplish any task in the task list. If so, return the task index; otherwise return 'no match'. Tasks: {}. This batch-style prompting significantly accelerates inference compared with querying each proposal independently.

7. Hyperparameter Sensitivity Analysis

τ_{match}	AP	AP ₅₀	AP ₂₅
0.6	26.4	38.3	46.4
0.5	28.2	39.6	47.9
0.4	28.6	40.5	48.8
0.3	27.3	38.2	45.9

Table 7. Sensitivity analysis of the τ_{match} parameter on subsets of the ScanNet200 validation set.

τ_{exp}	AP	τ_{vis}	AP	γ	AP	τ_{merge}	AP
0.00	28.0	0.1	28.6	0.5	27.6	0.8	27.6
0.03	28.2	0.2	29.1	0.4	28.6	0.7	28.4
0.05	28.6	0.3	27.2	0.3	28.6	0.6	28.6
0.07	28.0	0.4	24.9	0.2	27.0	0.5	27.0

Table 8. Sensitivity analysis of hyperparameters in the Proposal Refinement module on subsets of the ScanNet200 validation set.

K	ScanNet200			SceneFun3D	
	AP	AP ₅₀	AP ₂₅	AP ₅₀	AP ₂₅
1	28.6	40.5	48.8	9.8	20.6
2	28.8	40.8	49.0	10.2	20.8
3	28.9	41.8	49.5	10.5	21.2

Table 9. Ablation study on the MLLM top- K parameter on subsets of the ScanNet200 and SceneFun3D validation sets.

We analyze the sensitivity of key hyperparameters used in our framework. As shown in Tab. 7 and Tab. 8, the results remain stable across a wide range of values in both the Proposal Generation and Proposal Refinement modules.

We also evaluate the effect of varying the MLLM top- K parameter, as summarized in Tab. 9. Larger K generally improves performance but increases inference latency; in practice, users can choose an appropriate trade-off based on computational constraints.

8. Runtime Analysis

We analyze the runtime of our framework and compare it with the previous state-of-the-art, DetailMatters [15]. Most of our runtime is spent on model inference. The cost of the 2D open-vocabulary segmenter and DINO scales with the number of video frames, while the proposal-classification cost (via either MLLM or CLIP [28]) mainly depends on the number of proposals.

DetailMatters [15] follows the Open3DIS [23] pipeline and employs Grounding-DINO [20] as its 2D open-vocabulary detector. Because our method additionally incorporates a DINO [25] model, we choose to pair it with a more lightweight 2D open-vocabulary detector, YOLO-World [3], to balance the runtime overhead. As shown in Tab. 10, despite using one additional model, our overall runtime is approximately half that of DetailMatters.

The gap becomes even more pronounced in the proposal-classification stage. DetailMatters extracts the top 20 images for each proposal and applies multi-scale cropping, re-

	2D OV-SEG	DINO	Frames	Total
DetailMatters [15]	1.4	-	346	484
Ours	0.52	0.25	346	266

Table 10. Runtime of the 2D open-vocabulary segmenter and DINO. We report the per-frame runtime (in seconds), the average number of frames per scene, and the average runtime per scene on the ScanNet200 validation set.

	Classification	Proposals	Total
DetailMatters [15]	5.9	56	330.4
Ours ($K=3$)	1.6	56	89.6
Ours ($K=1$)	1.1	56	61.6

Table 11. Runtime of the proposal-classification stage. We report the per-proposal runtime (in seconds), the average number of proposals per scene, and the average runtime per scene on the ScanNet200 validation set.

sulting in roughly 60 Alpha-CLIP [34] forward passes per proposal, in addition to substantial preprocessing overhead. In contrast, our pipeline directly overlays a red bounding box on the original image to highlight the target and only feeds the top 3 images into the MLLM. As shown in Tab. 11, our approach achieves substantially lower inference latency compared to DetailMatters.

For fairness, all reported DetailMatters timings are obtained from our custom re-implementation, and are generally lower than the values reported in the original paper due to differences in implementation and hardware.